

Multiplexed temporally focused light shaping for high-resolution multi-cell targeting: supplementary material

NICOLÒ ACCANTO^{1†}, CLÉMENT MOLINIER^{1,2†}, DIMITRII TANESE¹, EMILIANO RONZITTI^{1,2}, ZACHARY L. NEWMAN³, CLAIRE WYART⁴, EHUD ISACOFF^{3,5,6}, EIRINI PAPAGIAKOUMOU^{1,7} AND VALENTINA EMILIANI^{1*}

¹Wavefront-Engineering Microscopy group, Neurophotonics Laboratory, CNRS UMR8250, Paris Descartes University, 45 rue des Saints-Pères, Paris, France

²Sorbonne Université, CNRS, INSERM, Institut de la Vision, 17 Rue Moreau, 75011, Paris, France

³Department of Molecular and Cell Biology, University of California, Berkeley, Berkeley, California, USA

⁴Institut du Cerveau et de la Moelle épinière (ICM), Sorbonne Universités, UPMC Univ. Paris 06, Inserm, CNRS, AP-HP, Hôpital Pitié-Salpêtrière, Boulevard de l'hôpital, F-75013, Paris, France

⁵Helen Wills Neuroscience Institute, University of California, Berkeley, California, USA

⁶Physical Bioscience Division, Lawrence Berkeley National Laboratory, Berkeley, California, USA

⁷Institut national de la santé et de la recherche médicale (Inserm), Paris, France

[†]Equally contributing authors.

*Corresponding author: valentina.emiliani@parisdescartes.fr

Published 19 November 2018

This document provides supplementary information to "Multiplexed temporally focused light shaping for high-resolution multi-cell targeting," <https://doi.org/10.1364/optica.5.001478>.

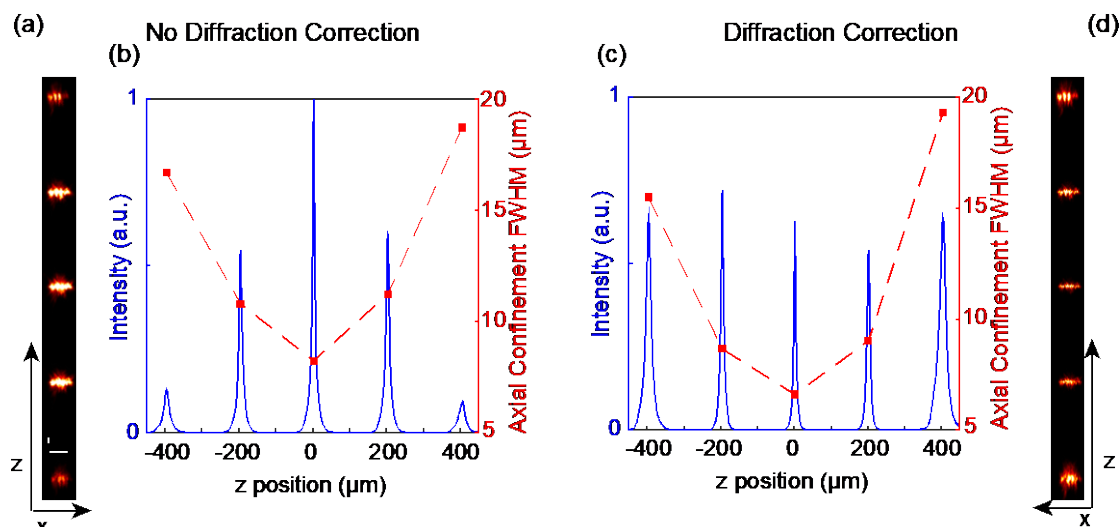


Figure S1. Characterization of holographic spots in z. (a) x - z view of 7 holographic spots (15 μm in diameter) placed one on top of the other, at relative distances of 200 μm in z . No diffraction-efficiency correction was applied in the experiment. Scale bars: 15 μm . In order to properly visualize the image the pixel are not square, which is why the scale bars have different lengths in z and x for the same real length of 15 μm . Note that, as a consequence of the lower diffraction efficiency of SLM2 when making spots out of the centre of the FOE, the spots are less intense as one moves away from the central position. (b) Intensity profiles (blue curves) and axial confinement (red filled squares) for the 7 spots in (a). One can notice the lower signal produced by the spots far from the centre. The second notable effect is the degradation of the axial confinement as one moves away from $z=0$. The dashed line is a guide to the eye. (c) Same as (b) but when diffraction efficiency correction was applied. We could correct for the lower signal and produce spots with similar maximal intensity in region from (-600 to 600 μm) in z . (d) Same as (a) but when the diffraction-efficiency correction was applied. Without saturating the image one sees all the 7 spots at the same time with similar intensity.

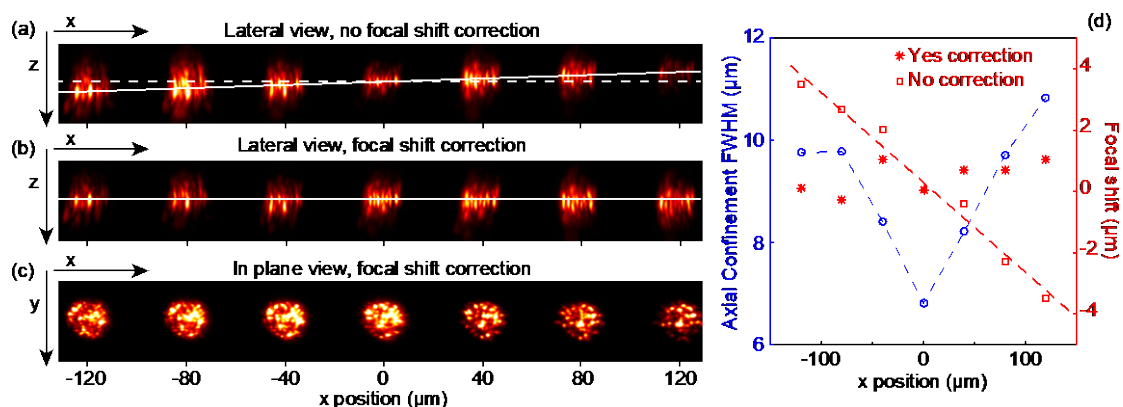


Figure S2. Characterization of holographic spots in the TF direction (x axis). (a) x - z view of 7 holographic spots (15 μm in diameter) placed in a line along the TF direction (x axis) at relative distances of 40 μm . Two effects are visible: i) the axial confinement got worse when approaching the edges of the FOE in x ; and ii) the focal position was not exactly the same for all the spots but shifted linearly, as indicated by the solid line. As the latter effect was not observed in the y direction (i.e. the direction perpendicular to TF, see **Supplementary Figure 3**), we attribute this to spectral frequencies dispersion by the diffraction grating, which in turns caused an asymmetry at the position of SLM2 (spectral frequencies were dispersed in the x but not in the y direction). This is similar to pulse-shaping setups, in which the separation of the spectral frequencies at the SLM gives the possibility to change the time profile of the laser pulse. However, contrary to what is commonly done in a pulse shaping experiment, in this case we were not correcting for the intrinsic wavelength dependence of SLMs. We can then speculate that our system likely introduced spatio-temporal coupling effects, which might be the cause of the axial shift. An improvement of the current setup will therefore consist in a systematic study of this possible spatio-temporal effects, in order to get advantage from the double regime that the SLM2 operates with, i.e the spatial and time domain. (b) Same as (a) but after correcting the focal shift holographically, i.e. by introducing an opposite focal shift with the SLM. The white solid line indicates the new focal plane of the spots. (c) x - y view of the 7 spots. (d) Behaviour of the axial confinement (blue circles) and the focal position for the 7 spots before (red squares) and after (red crosses) focal shift correction. Indeed, the focal position shifts linearly with the x coordinate when no correction is applied. The red dashed line is a guide to the eye.

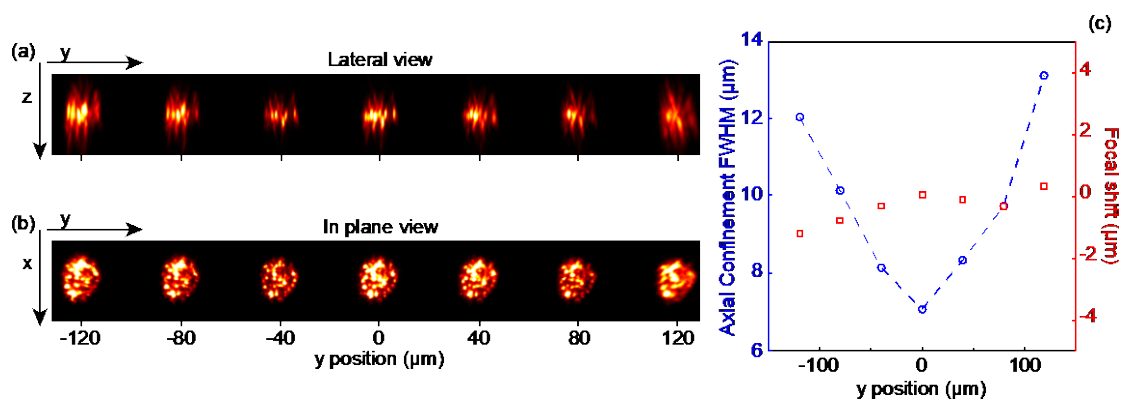


Figure S3. Characterization of holographic spots in the perpendicular to TF direction (y axis). (a) y - z view of 7 holographic spots ($15\ \mu\text{m}$ in diameter) placed in a line along the direction perpendicular to TF (y axis) at relative distances of $40\ \mu\text{m}$. The axial confinement got worse close to the edges of the FOE in y . In contrast to the TF direction, in this case all the spots focused in the same z position. (b) x - y view of the 7 spots. (c) Behaviour of the axial confinement (blue circles) and the focal position (red squares) for the 7 spots. The axial confinement was worse at the edges of the FOE, while the focal position was the same for all the spots.

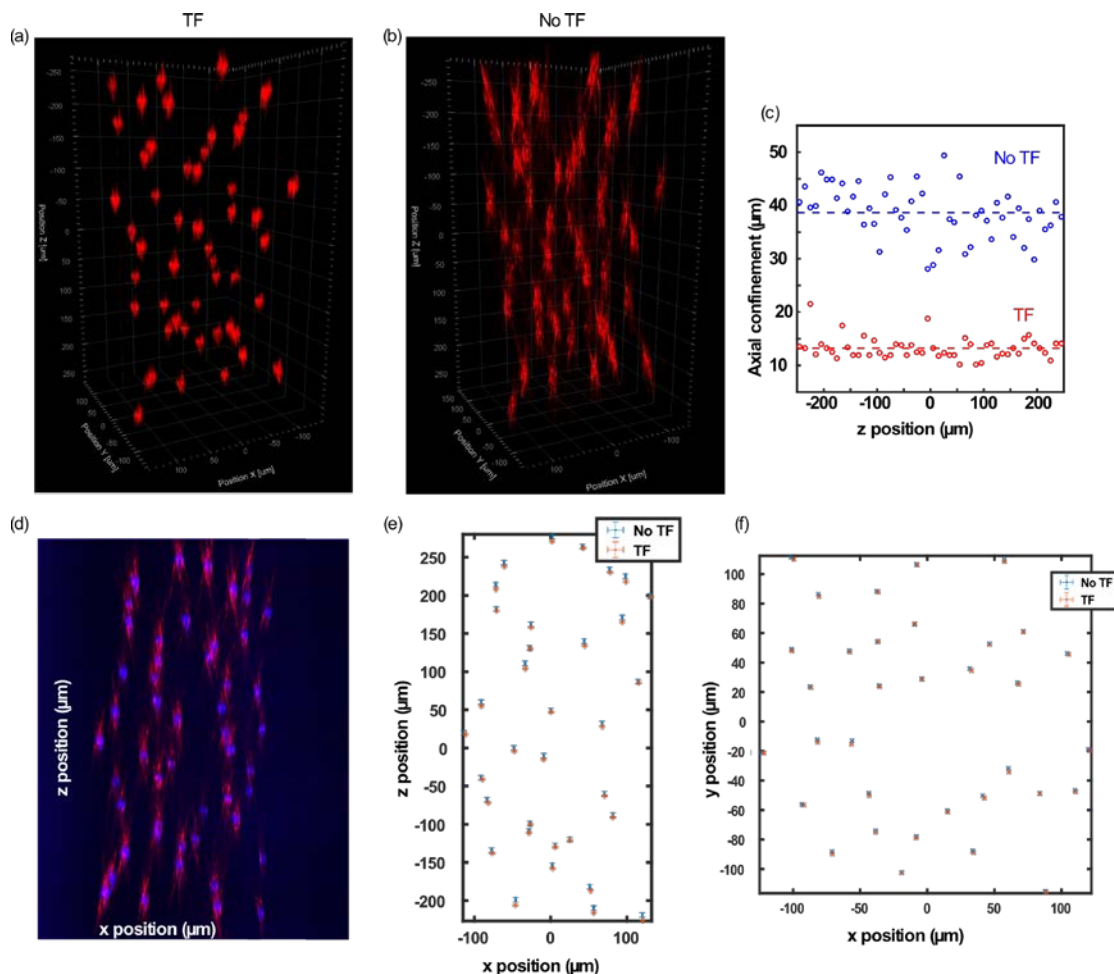


Figure S4. Comparison of 3D-CGH-TF with and without TF. (a) 2PE fluorescence volume representation of 50 holographic temporally-focused circular spots of 15 μm diameter, each of them lying on a different plane, in a volume of $300 \times 300 \times 500 \mu\text{m}^3$. The experimental procedure was the same as the one for Fig. 2 of the main manuscript. (b) Same as (a) but without TF. In this case the diffraction grating for dispersing the spectral frequencies and performing TF was replaced by a mirror. Significant increase in axial resolution when TF was applied, allowed us to better distinguish neighbouring holographic spots in the 3 directions. (c) Axial confinement, calculated as the FWHM of the axial intensity profile of each spot, as a function of the z position for the TF case (red symbols) and no TF (blue symbols) case. The red and blue dashed lines represent the mean FWHM for the two cases which was $\sim 13 \mu\text{m}$ in the TF case and $\sim 38 \mu\text{m}$ in the no TF case. (d) Superposition of TF (red) and No TF (blue) projection in the xz direction. (e) Manual estimation of the centre of the spots in (d) with error bar of 1 μm in x and 1 μm in z for TF (red) and 1 μm in x and 3 μm in z for No TF (blue). In the case of No TF the 3 μm comes from the uncertainty in determining the precise focal plane for each spot. (f) Same as (e) but in xy direction. The errors given are 1 μm in both directions. We observe that, despite the spatial chirp introduced by the grating, the final distribution of spots is very similar.

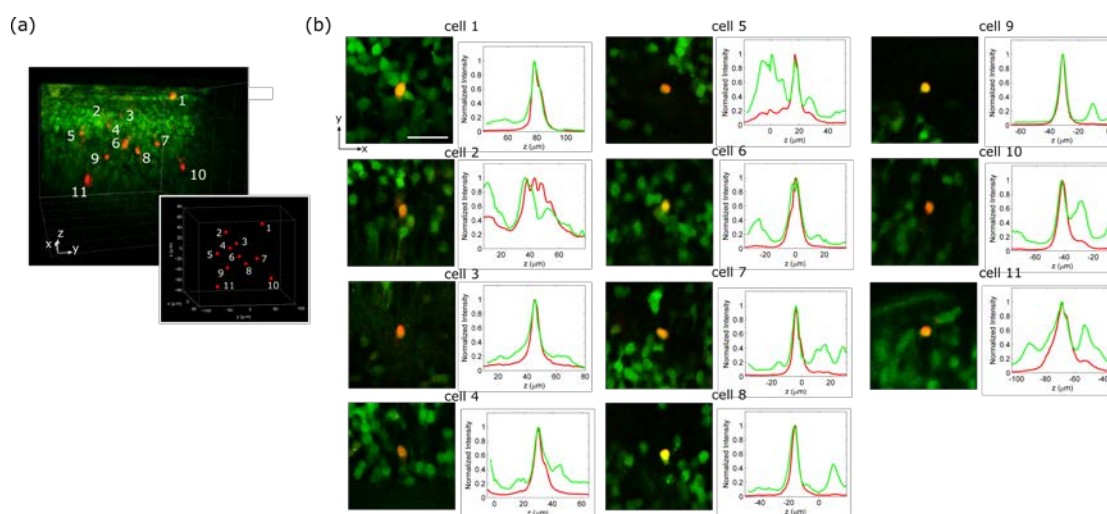


Figure S5. Simultaneous photoconversion of an ensemble of kaede expressing neurons. (a) 3D view of a 2P stack merging green and red fluorescence after targeted simultaneous 2P photoconversion of a set of 11 neurons (also shown in Fig. 6 of the main manuscript). The inset represents schematically the position of the generated 3D MTF-CGH spots targeting single cells. Spots and the relative targeted cells are labeled with numbers. (b) Top view extracted from the 2P stack reported in (a), zooming on each targeted cells (scale bar: 20 μm), together with its corresponding normalized axial intensity profiles of green and red fluorescence. In addition to Figure 6 of the main manuscript, here we show the complete set of photoconverted cells. The cells labelled 1,2 and 3 in Fig. 6 correspond respectively to cells number 1,7 and 11 in this figure.

Supplementary Note: General alignment procedures

In all the configurations described in the main paper, there are two requirements that need to be precisely met when designing and aligning the system: (1) the diffraction grating has to be in a plane conjugated to the sample plane; (2) SLM2, placed after the diffraction grating, has to be in a Fourier plane of the diffraction grating and conjugated to the objective back focal plane.

It is then desirable to maximize the illumination at least of SLM1 (that of SLM2, as detailed in the paper, depends on the specific MTF-LS technique used), and to use the full NA of the microscope objective. This forces one to initially expand the laser beam to roughly the size of SLM1 and to choose the appropriate focal distances for the lenses (and grating) to fill the pupil of the objective at least in the TF direction.

In the MTF-CGH case one could start the alignment by replacing the diffraction grating with a mirror and with the SLMs switched off. In this way SLM1 is conjugated to SLM2 by means of a first telescope (L1 and L2 in Fig. 1(a)) and a second telescope (L3 and L4 in Fig. 1(a)) conjugates SLM2 to the back focal plane of the objective. Choosing a first 1 to 1 telescope ensures the correct illumination of both SLMs. The second telescope has to be chosen such that the de-magnified image of SLM2 slightly overfills the pupil of the objective. Generally speaking, choosing big diameter lenses with large focal lengths helps in minimizing the divergence of the laser beam on the optical table. Changing the mirror for the diffraction gratings then ensures the correct implementation of MTF-CGH. When using a static phase mask the alignment principle remains the same, only that one should take care in choosing the right telescope (L1, L2) to correctly image the phase mask on SLM2.

In the MTF-GPC case one should start by aligning the GPC interferometer. In this case SLM1 is conjugated to the diffraction grating plane (with the addition of the phase contrast filter-PCF in the Fourier plane). The PCF should be mounted on a xyz translation stage and placed at the focal distance of $L1^{GPC}$. Placing a camera at the focal position of $L2^{GPC}$, i.e. where the diffraction grating will then be placed, one should optimize the alignment of the PCF. Once this is done it is sufficient to guide the beam through the appropriate lenses at the center of SLM2 and of the objective pupil. For doing this, one should start with SLM2 off.

The MTF-MS case is similar to MTF-GPC, with the difference that one has to remove the PCF. Initially one should use SLM1 to make only one shape, e.g. a circle of half the size of the SLM1 and fill it with a prism effect encoding for a small displacement Δx in the horizontal direction. In this way, in the focus of $L1^{MS}$ there will be two diffraction-limited spots: one corresponding to the unshaped light (zero order) and the other coming from the chosen shape. One should use a beam stop to block the first diffraction-limited spot. In this way, after the lens $L1^{MS}$ there should appear the de-magnified image of the circle drawn by SLM1. The rest of the alignment consists in guiding such shape through all the lenses, at the center of SLM2 and the objective pupil.

To make n different shapes one should start by dividing SLM2 in n horizontal zones, applying to each of them a different phase (e.g. encoding n different shifts in the xy plane), and looking at the resulting pattern at the sample plane. One should then make n different shapes with SLM1, encoding them with a prism effect for the same displacement Δx in the x direction and a displacement Δy in the y direction, such as to fall in the n different regions of SLM2. This should ensure that each shape is correctly sent to a different area of SLM2. One should therefore see n different shapes appearing at different locations at the sample. Finally, varying the Δy such as to optimize the quality of the shapes and minimize the cross talk among them completes the alignment procedure.